

Development of an Optimized Induction Melting System for Fabricating Paraffin Fuel Grains for Hybrid Rocket Propulsion

José Refugio Martínez¹ , José Ángel de la Cruz-Mendoza² , Emmanuel Vázquez-Martínez² , Daniel Romero de la Cruz³ , Azdrubal Lobo Guerrero^{4,*} , Gerardo Saucedo-Zárate⁵ , José Luis Arauz-Lara² , Hernán González-Aguilar¹ , Gerardo Ortega-Zarzosa¹ 

1. Universidad Autónoma de San Luis Potosí  – Facultad de Ciencias – San Luis Potosí – México.

2. Universidad Autónoma de San Luis Potosí  – Instituto de Física – San Luis Potosí – México.

3. Universidad Autónoma de San Luis Potosí  – Facultad de Ingeniería – San Luis Potosí – México.

4. Universidad Autónoma del Estado de Hidalgo  – Instituto de Ciencias Básicas e Ingenierías – Área Académica de Ciencias de la Tierra y Materiales – Mineral de la Reforma – México.

5. Instituto Mexicano del Espacio Ultraterrestre – San Luis Potosí – México.

*Correspondence author: azdrubal_guerrero@uaeh.edu.mx

ABSTRACT

This work reports the development of an induction melting system for producing paraffin-based fuel units for hybrid rockets. The system is based in oscillating low-frequency magnetic field to generate heat within the material, enabling a precise temperature control through an on/off process. Additionally, the steel used as the material for fabricating the mold facilitates a slow cooling rate, leading to the formation of homogeneous paraffin fuel units free from cracks and microfractures, which is a critical requirement for their safe application in hybrid rockets and to ensure an efficient fuel combustion. The fabricated paraffin fuel units underwent rigorous characterization of their thermal, structural, and optical properties to ensure their suitability as fuel units in a hybrid rocket engine developed for the Mexican Cabo Tuna space program.


Keywords: Paraffins; Magnetic induction heating; Induction systems; Propellant grains; Hybrid propellant rocket engines.

INTRODUCTION

Rocket engines typically use either solid or liquid propellants. However, hybrid propulsion offers a unique combination of both systems. The development of hybrid rocket engines shows interesting advantages by utilizing a unique combination of solid fuel grains and gaseous or liquid oxidizer, overcoming some of the limitations inherent in traditional rocket engines. In hybrid rockets, propellants often comprise a solid fuel and a liquid or gaseous oxidizer. Notably, hybrid rockets boast improved safety compared to solid propellant rockets. This is because the oxidizer, a highly reactive component, is stored separately from the solid fuel until it is injected into the combustion chamber, minimizing the risk of accidental ignition.

While hybrid propulsion offers advantages over traditional solid and liquid propellant rocket engines (Casiano *et al.* 2010; Caveny *et al.* 2003; Okninski 2018; Oztan and Coverstone 2021; Sackheim 2006), its development has been hindered by challenges associated with these propellants. In this context, paraffin wax emerges as a promising fuel option for hybrid engines, but its use in launch applications requires a more comprehensive characterization of its structural integrity (Mazzetti *et al.* 2016; Veale *et al.*

Received: July 04, 2024 | Accepted: Sept. 17, 2024

Section editor: José Rocco 

Peer Review History: Single Blind Peer Review.



2017; 2018; 2021). Within the Mexican Cabo Tuna space program (Saucedo-Zárate *et al.* 2022a; b), there is a project focused on developing a hybrid propulsion system using nitrous oxide as the oxidizer component and paraffin wax as the solid fuel.

Paraffin-based fuels are the next step for improving the performance of hybrid rocket motors, offering low obtention costs and improved performance due to their favorable thermal properties. This readily available organic material holds potential not only in the development of fuel grains for hybrid rockets but also in energy storage systems (Karabeyoglu *et al.* 2001; Leccese *et al.* 2019). Paraffin is an odorless, tasteless, waxy solid. It melts from 23 to 67 °C and is unaffected by the most common chemical reagents but burns readily in the air (Abhat 1983). Paraffin wax is representative exponent of a typical phase-change material due to its large latent heat and stable phase change. The paraffin chemical bonds break up when its temperature increases, leading to a phase change from solid to liquid (Alkan 2006). This process is endothermic, meaning paraffin absorbs heat from the surrounding environment. Then, after storing heat, the paraffin melts when the phase change temperature is reached (Sharma and Sagara 2005).

Paraffin wax is made from long chains of hydrocarbons that remain solid at room temperature. Chemically, paraffin wax is a mixture of high molecular weight alkanes with the general formula C_nH_{2n+2} , where n is an integer number from 22 to 27. Paraffin is chemically stable, having no tendency to segregate, with high heat of fusion and non-reactivity (Mansoori *et al.* 2003). Beyond its inherent advantages (non-toxic, non-hazardous, easily shippable, low-cost, and potentially reusable), paraffin wax presents some benefits when used as a solid fuel in a hybrid rocket due to its high performance with nitrous oxide. This makes paraffin wax a highly desirable propellant choice (Kobald *et al.* 2018; Thomas *et al.* 2021). Despite its advantages, paraffin wax also presents some weaknesses. In its solid state, it shows low thermal conductivity, is flammable and has poor mechanical strength, making it necessary to design of special containers to alleviate the lack of structural strength in aerospace applications (Hasnain 1998; Hiran *et al.* 1994). Furthermore, tight-tolerance processing of paraffin wax involves a complex challenge due to its high shrinkage rate from 15 to 25% (Karabeyoglu *et al.* 2004). In addition, the solidification process can introduce grain deformations, internal stresses, rips, defects, and microcracks, creating microstructural discontinuities, which change the combustion behavior of the paraffin wax. Therefore, this inhomogeneity is undesirable for its application as a fuel for launching rockets equipped with hybrid engines. Achieving high structural uniformity in the fabrication of paraffin-based solid fuel grains is a pending task.

Solid fuel grains with an annular central port can be fabricated from paraffin wax using both laboratory and industrial-scale manufacturing techniques. The lab-made model uses a configuration consisting of a circular mold and a piston. This piston applies a mechanical force to counteract the volumetric shrinkage experienced by paraffin wax during its transition from liquid to solid (Bernard *et al.* 2013; Piscitelli *et al.* 2018). However, higher-scale fabrication uses a spin-casting machine. In this case, a variable rotational speed allows for control over the centrifugal forces acting on the molten paraffin wax during its solidification (Mahottamananda and Kadiresh 2019; Piscitelli *et al.* 2015; Tang *et al.* 2017). On the other hand, paraffin donuts used as fuel are usually fabricated by a mechanical process or by melting paraffin into a mold. In this case, the paraffin wax forms a thin hydrodynamically unstable liquid layer. Other mechanical techniques based on die casting and centrifugal casting have been used (Masato *et al.* 2017; Stober *et al.* 2021). Paraffin wax fuel grains typically fabricated using a heating and cooling process to induce a solid-to-liquid phase transition, are susceptible to conducive to the formation of cracks and microcracks within the paraffin grains. Thus, eliminating these defects during the fabrication of paraffin-based fuel grains with specific geometries is crucial for hybrid combustion. Cracks and other imperfections can lead to combustion instabilities, highlighting the importance of a defect-free manufacturing process. Additionally, paraffin wax has poor mechanical strength, making it susceptible to structural deformation during various stages like fabrication, casting, handling, and transportation. A surge in research activity has recently focused on enhancing the mechanical properties of paraffin-based fuels. This is being achieved through the incorporation of energetic additives and reinforcing frameworks (Bisin *et al.* 2020; Pal *et al.* 2021; Risha *et al.* 2007). Polyethylene, carbon black, ethylene-vinyl acetate, boron, aluminum, and nano-metallic additives improve the mechanical strength and combustion efficiency of paraffin fuel units (Kim *et al.* 2015; Kumar and Ramakrishna 2016). However, additives can diminish the positive effect of paraffin wax as a high regression rate fuel.

This work presents a novel system designed to manufacture paraffin fuel units conforming the requirements of the hybrid rocket engine employed in the Mexican Cabo Tuna space program. The system explores the application of the induction heating principle as a promising alternative for fabricating paraffin wax fuel grains for hybrid rocket motors. Furthermore, the system

facilitates the technical evaluation of paraffin units due to the absence of aggregates. Notably, the design allows for scalability to produce paraffin units in various geometries and explore the effects of additive incorporation. Induction heating, commonly used in high-temperature metal melting applications, relies on the application of strong magnetic fields. In contrast, our design utilizes an oscillating low magnetic field to generate heat within a safe physiological range, specifically tailored for paraffin wax melting. This enables the fabrication of paraffin fuel units with a donut shape, free of structural defects like cracks or air bubbles, and with enhanced mechanical properties, suitable for use in hybrid motors of suborbital rocket vehicles.

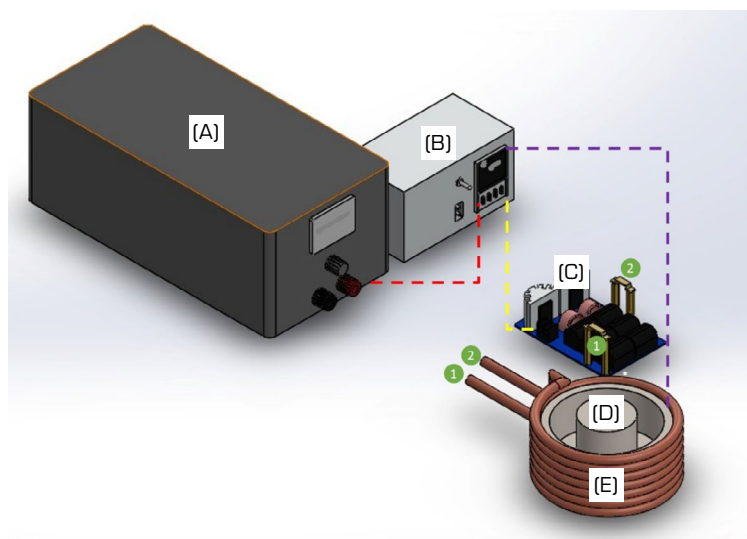
Crack formation typically arises due to thermal shrinkage of the paraffin grain during cooling, resulting in elevated hoop stresses. Our system employs strict temperature control during melting. Notably, to the best of our knowledge, this is the first work utilizing an induction system for the specific purpose of fabricating paraffin wax fuel for hybrid rockets. Beyond its novelty, the system offers a simple, cost-effective, and efficient approach to producing high-quality, homogeneous paraffin donuts for this application.

Experimental

The fuel grains were fabricated from microcrystalline paraffin wax (Micro Shell Imp, CAS 64742-60-5), purchased from a local supplier. The paraffin consists of a complex combination of hydrocarbons obtained by treating petroleum microcrystalline wax with hydrogen in a catalyst. Paraffin is formed from long-branched chains of hydrocarbons with carbon numbers mainly from C_{25} to C_{50} .

Our hybrid rocket can accommodate cylindrical fuel grains with a height of 87 mm and a diameter of 132.2 mm. These grains have a central cylindrical hole with a diameter of 42.05 mm.

The induction melting system was specifically designed to fabricate paraffin fuel units with the required specifications for our hybrid rocket. Figure 1 depicts a melting system using a cylindrical steel mold (D) aligned with a coil (E). This coil connects to a zero-voltage-crossing oscillator (B), creating an oscillating circuit (C) that generates a magnetic field in the kHz range. This system can reach 100 °C within 30 minutes. The induction melting system was characterized using magnetic and temperature sensors.



Source: Elaborated by the authors.

Figure 1. Diagram of the induction melting system used to manufacture paraffin grains for use as the solid fuel component in hybrid combustion.

The structural behavior of molten and raw paraffin wax was analyzed by X-ray diffraction (XRD) and Fourier transform infrared spectroscopy (FT-IR). The X-ray patterns were obtained using an Inel Equinox 2000 diffractometer with a cobalt source ($\lambda = 1.7890 \text{ \AA}$) in the Bragg-Brentano geometry from a 10° to 60° diffraction angle and steps of 0.02° . The IR was carried out with a Bruker Vertex 70 FT-IR using diffuse reflectance mode. Thermal properties were analyzed by DSC measurements performed with a TA-Instruments series TSC Discovery at a constant rate of $10 \text{ }^\circ\text{C}/\text{minute}$ inside the differential thermal analysis (DTA)

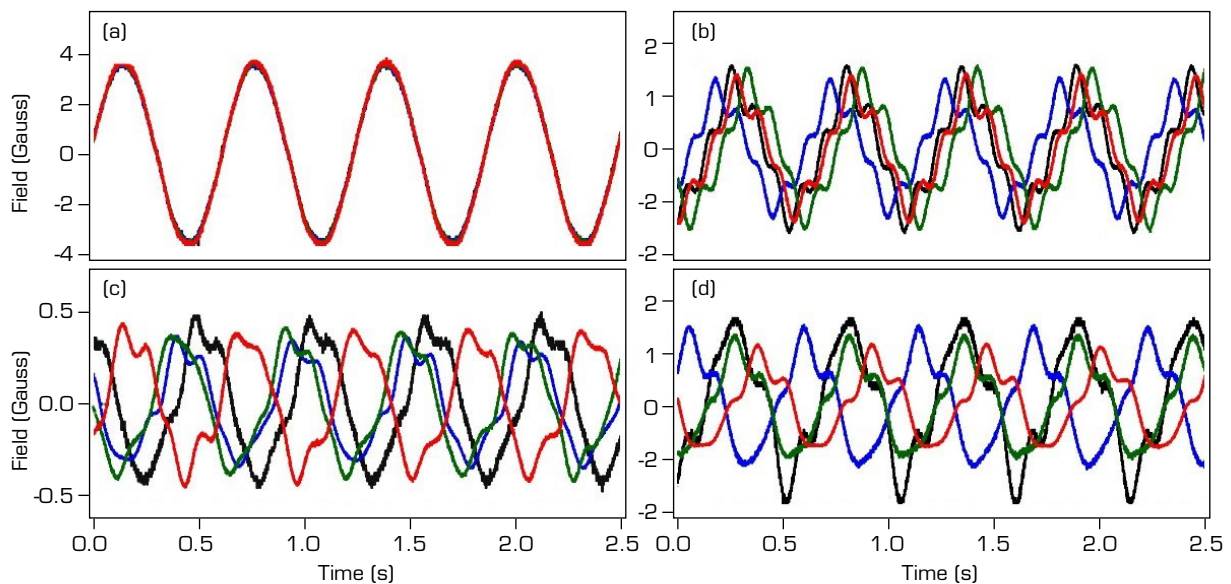
in an oxygen atmosphere up to 150 °C. Additionally, optical properties were analyzed with a Perkin Elmer LS55 fluorescence spectrophotometer using an excitation wavelength of $\lambda_{\text{ex}} = 317$ nm. Pressure tests were performed using a homemade mechanical pressure machine that utilizes a force sensor from Pasco, CI6746 economy force sensor (-50 N to 50 N). Surface analysis of the solid grains of paraffin was examined using a LEICA MZ-12x optical microscope with 50x and 500x magnifications, illuminated by a 650 nm line laser with power < 500 mW and a 532 nm laser with power < 1,000 mW.

RESULTS

Characterization of the induction melting system

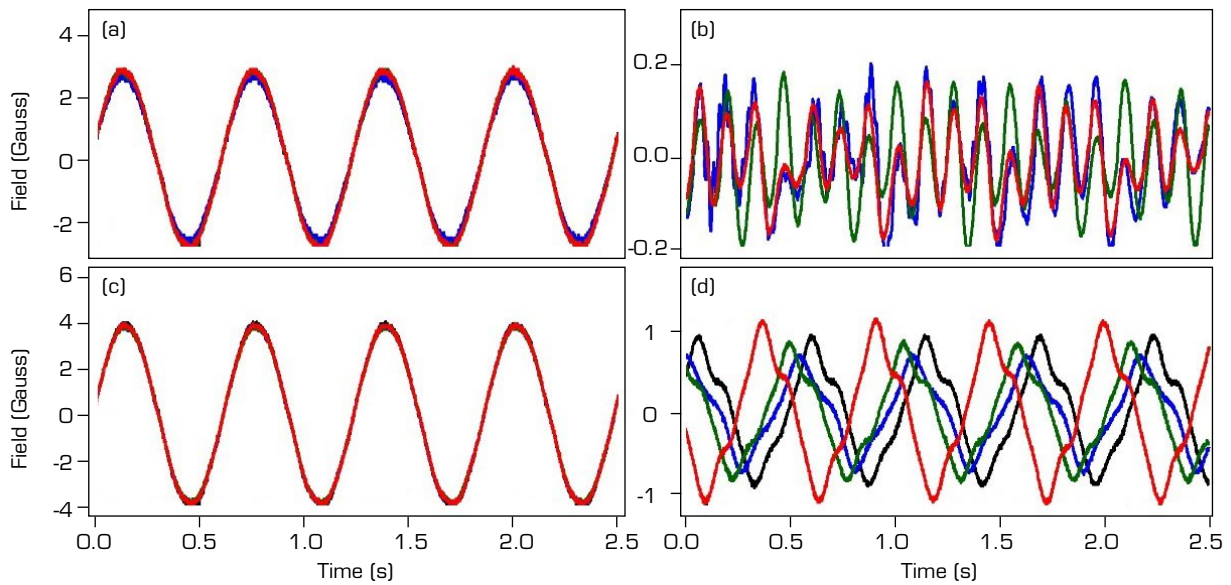
The induction melting system shown in Fig. 1 consists of a cylindrical coil made from a flexible copper tube of 9.25 mm (3/8"). The coil has a height of 8.5 cm, a 16 cm internal diameter, and seven turns (E). The coil is powered by a zero-voltage-crossing oscillator module (C). In a close-loop scheme, the oscillating circuit (E + C) can generate a magnetic field in the kHz range, which induces a temperature increase to 100 °C in 30 minutes. The close-loop scheme comprises an oscillator circuit, a power source (A), and a temperature control (B). This configuration is required for our application within the desirable temperature range. The copper coil is placed around the steel mold, with a heating volume of 1.709 cm³ (D), where the raw paraffin is melted. The coil was connected to the low-voltage and high-frequency (1000 W, 20 A, 12 to 48 V) oscillator (plugs 1 and 2).

Figures 2 and 3 show the axial and tangential magnetic fields measured inside of the mold. Additionally, measurements without the mold were performed to evaluate the effect of the steel mold. The magnetic field was measured at four points: (i) inside of the coil at the top, (ii) at the bottom, (iii) close to the coil, and (iv) at the center. Figure 2a shows the magnetic field measurements performed without the steel mold, revealing similar signals at the four points, except for one, due to the loop geometry presenting a small variation at the point where the loop begins and ends. Measurements with the steel mold are shown in Figs 2b-d. Figure 2b shows the magnetic field signals measured with the mold in place, but without the metal cover or the inner cylinder. Figure 2c shows the effect of adding the metal lid of the inner container and Fig. 2d shows the magnetic field signal of the fully assembled mold, including the cover and the inner cylinder.



Source: Elaborated by the authors.

Figure 2. Magnetic field signals obtained from four points (color lines) measured inside of the mold, near the end of the coil for (a) without the steel mold, (b) with the basic mold in place, (c) basic mold with its cover, and (d) with the complete mold.

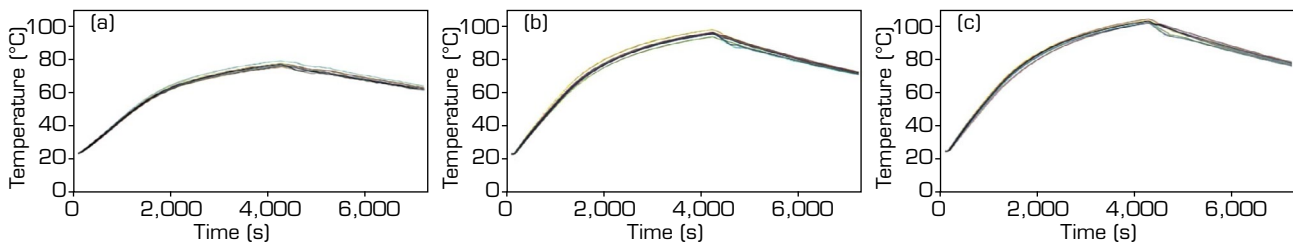


Source: Elaborated by the authors.

Figure 3. Signals of the magnetic field for four equidistant points (a) at the bottom near the end of the coil without the mold, (b) at the same points as (a) but with the mold, (c) coil without mold in the center, and (d) in the center with the mold.

The magnetic field signal's shape and intensity change when the different mold elements are added. This is caused by the magnetic field's interaction with the steel of the mold. Furthermore, the change in the signal's shape from sinusoidal to other forms is related to a rising temperature inside the mold. This effect is utilized to create the donut-shaped paraffin. Figure 2b shows that the intensity of the magnetic field in the system with the mold is about 25% compared to the one without the mold, and a phase shift is observed at the measurement points. Figure 2c shows that the shape of the magnetic field is altered when the lid of the inner container is added, and its intensity diminishes. Finally, the magnetic field for the completed mold is shown in Fig. 2d. In this case, the magnetic field intensity increases due to the presence of the inner cylindrical metal core. Similar measurements were obtained at points near the coil and at the center (both top and bottom) because the radial magnetic field is constant. However, there is a reduction of the magnetic field at the bottom of the coil in the vertical direction. These results demonstrate that the system can achieve the necessary temperature to melt raw paraffin, resulting in the paraffin fuel grains upon solidification.

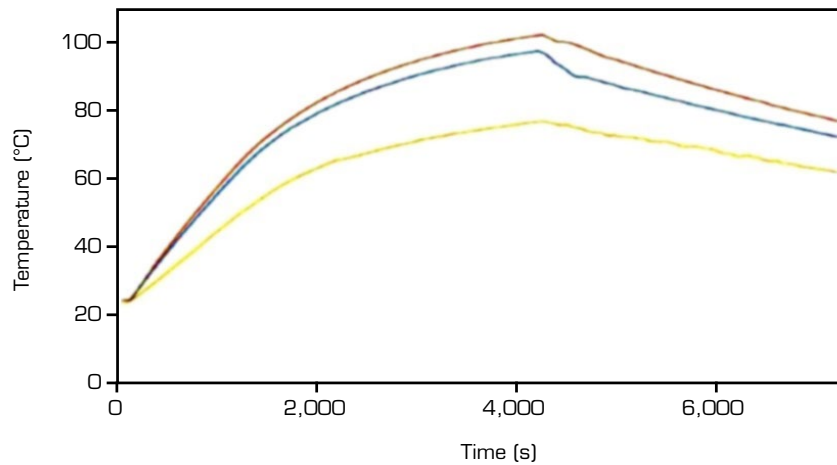
Figure 4 shows the temperature measurements obtained from sensors located at different points inside of the mold during the heating and cooling cycle. We observed a low-temperature dispersion at the bottom of the mold, with about eight degrees difference for the middle and top, and the maximum temperature diminished as the mold height increased.



Source: Elaborated by the authors.

Figure 4. Temperature measured in the interior of the mold at eight points: (a) on the top, (b) in the middle, and (c) on at the bottom.

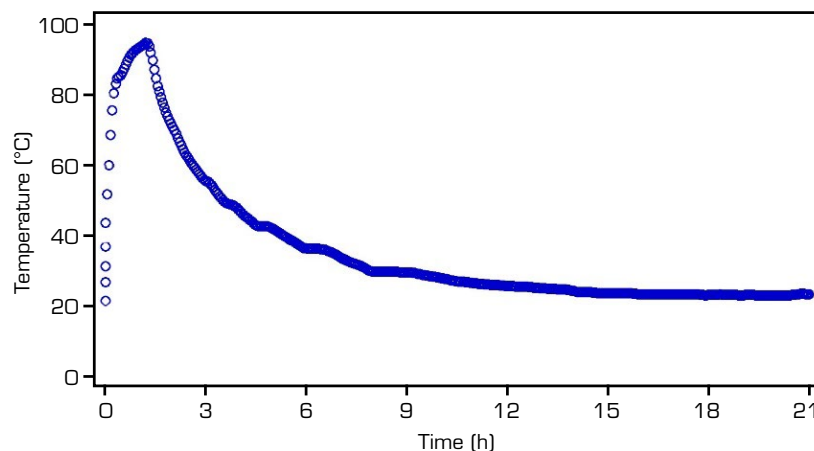
Figure 5 shows temperature measurements in three higher positions, where the interaction with the ambient is greater. In this case, the temperature increases more slowly than recorded at the bottom or in the middle regions. In the higher region, a temperature of 77 °C is reached in 4,100 seconds, compared with 97 °C and 101 °C reached in the middle and bottom regions. Therefore, the temperature range reached by induction in the steel mold corresponds to the melting temperature of raw paraffin, allowing the system to be used for the fabrication of paraffin grains for its use as solid fuel for the hybrid rocket motor.



Source: Elaborated by the authors.

Figure 5. Temperature records at the top, middle, and bottom regions of the fully assembled steel mold.

In the system with raw paraffin, the magnetic field was adjusted to 30 kHz, and the temperature was controlled by a sensor located in the mold. After 1.4 hours, the temperature reached 100 °C, and the paraffin was completely melted inside the mold. Then, the system was turned off and left to cool under ambient conditions. The cooling process is slow, and 20 hours later, the paraffin reaches the room temperature. Figure 6 plots the temperature profile of the process followed by the paraffin. As seen, the temperature increases up to 100 °C and subsequently decreases when the magnetic field is turned off. The slow cooling process of the system prevents disturbances in the material during solidification. According to the results, solidification starts at the top of the paraffin, forming star-shaped solid rings until a homogeneously solidified paraffin unit is obtained.

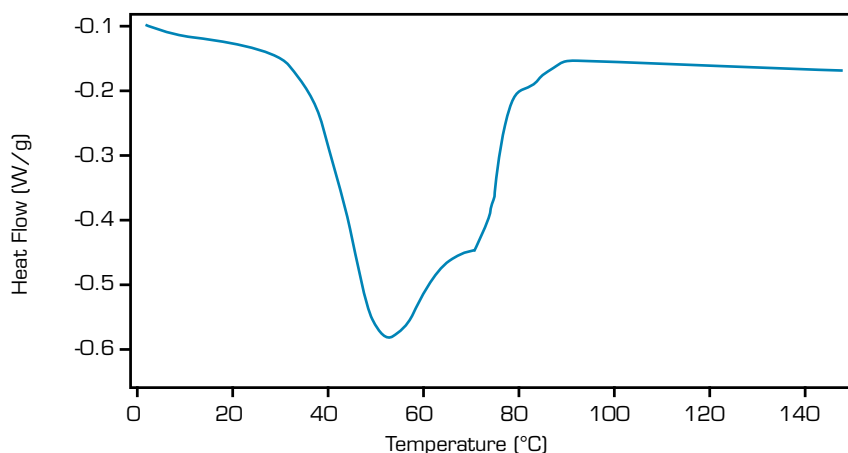


Source: Elaborated by the authors.

Figure 6. Heating and cooling temperature profile of the raw paraffin.

Characterization of the paraffin fuel unit

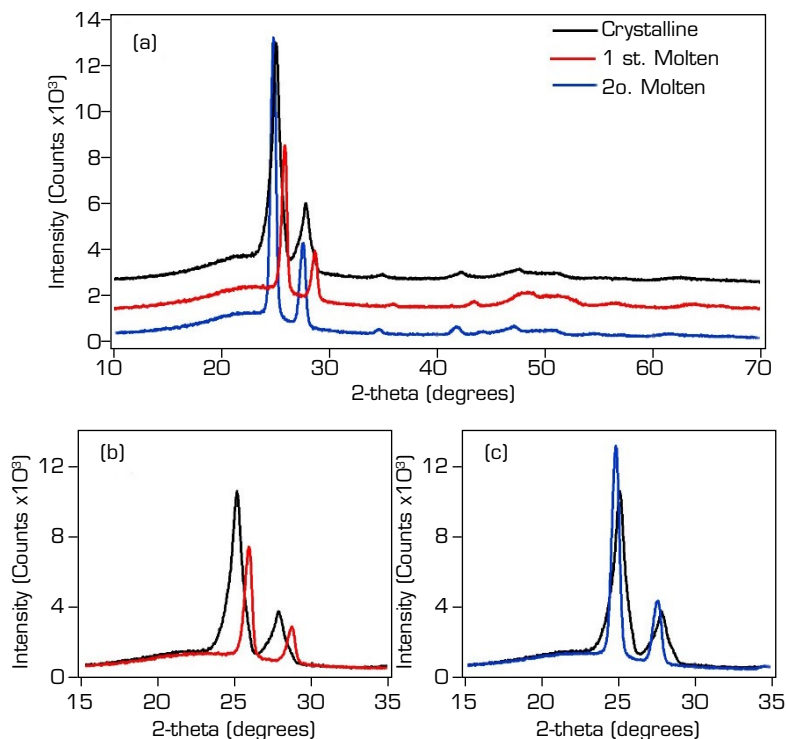
Figure 7 displays the DTA of the microcrystalline paraffin wax, showing one peak with two shoulders in the temperature range from 30 to 90 °C. These analyses indicate that paraffin wax, at atmospheric pressure, is completely melted at 85 °C. The peaks are interpreted as the solid-liquid phase transition. The manufactured paraffin grains exhibited an initial melting point of 52.8 °C and presented a melting enthalpy of 160.3 J·g. As there is no small peak below 53 °C, we can confirm that the solid-solid phase transition below the main melting temperature (referred to as the melting temperature hereinafter) of the larger peak is not present. The commercial paraffin wax did not show significant degradation in thermal properties after repeated 1,500 melting-cooling cycles.



Source: Elaborated by the authors.

Figure 7. DTA measurement of the microcrystalline commercial paraffin wax.

Figure 8a shows the experimental X-ray pattern for the raw paraffin (crystalline), the molten paraffin using our induction system, and one sample molten twice in the same system. The main difference in the X-ray diffractograms corresponds to a shift of the semicrystalline peaks for molten paraffin to higher diffraction angles. Additionally, the semi-crystallinity of the paraffin structure is recovered in the paraffin molten twice, as observed in Figs. 8b and c for the paraffin molten two times. The solid-solid phase transition is not observed in the differential scanning calorimetry (DSC) curves but is evident in the X-ray patterns. After the first melting process, the cooling gives one of the solid phases associated with the number of C and H atoms in the paraffin. In contrast, the second melting process results in another solid phase after cooling.



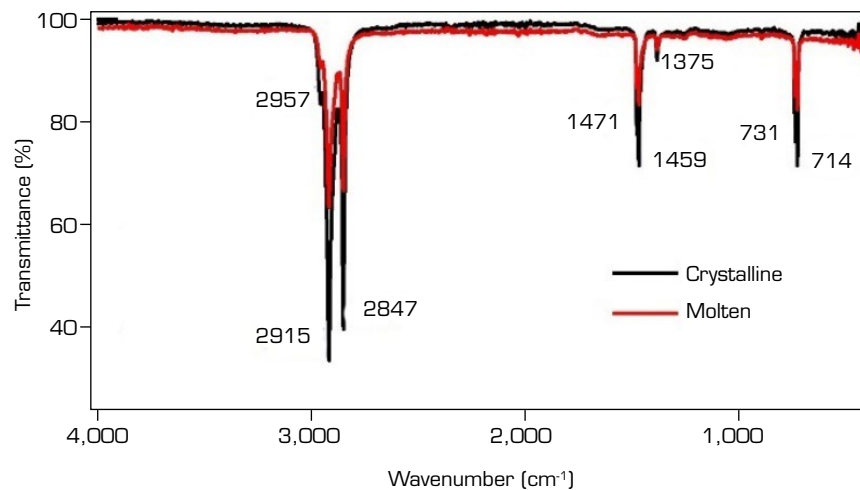
Source: Elaborated by the authors.

Figure 8. Experimental X-ray patterns obtained from the raw paraffin, and the paraffin subjected to a one and two melting processes (a). Comparison between the raw paraffin and the molten paraffin (b) and the raw paraffin and the paraffin molten twice (c).



Previous works reported that paraffin transitions to a different solid phase after the cooling process (Piscitelli *et al.* 2018). A detailed analysis of the structural behavior of paraffin under the heating-cooling process needs to be discussed in future works. The phases of the paraffin may include the following: n-nonacosane, $C_{29}H_{60}$ (40-1997); n-heneicosane, $C_{21}H_{44}$ (31-1705); n-tricosane-n-pentacosane, $C_{23}H_{48}$, $C_{25}H_{52}$ (53-1798); n-tricosane, $C_{23}H_{48}$ (43-1854); and n-pentacosane, $C_{25}H_{52}$ (53-1793) (Bucio *et al.* 2021; Gulfam *et al.* 2019; Wunderlich *et al.* 2003). The degree of crystallinity for the first molten process is lower than for the second molten process, which is longer for the raw paraffin (Lee *et al.* 2010; Ryan *et al.* 1997). Additionally, the highest diffraction intensities of paraffin are related to the presence of straight alkanes (C_nH_{2n+2}) (Dorset 1995). Linear alkanes exhibit more crystallinity than nonlinear alkanes (Dorset 2005). Moreover, as it was observed in paraffin with varying crystallinity, achieving a high degree of crystallinity generally requires more energy for solid-liquid transitions (enthalpy of fusion).

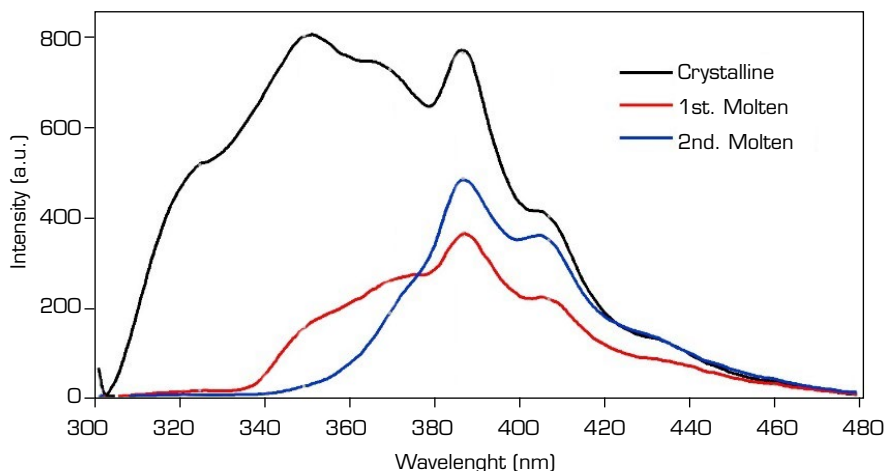
The chemical behavior of the raw paraffin (crystalline) and the paraffin obtained after melting in our induction system is analyzed using the FT-IR spectra in Fig. 9. The paraffin spectra reveal the presence of carbon-hydrogen stretching and bending absorption bands from 1,000 to 3,000 cm^{-1} . The symmetric carbon-hydrogen bending absorption of the CH_3 group at 1,375 cm^{-1} , the CH deformation around 1,459 cm^{-1} , and the CH_2 rocking absorption band at 888 and 731 cm^{-1} confirm the linear saturated aliphatic structure of the paraffin (Cho and Fogle 1999; Varshney *et al.* 2012). The FT-IR spectrum of the paraffin molten by induction confirms the absence of any oxygen bands (Vyshniak *et al.* 2018). The band at 1,471 cm^{-1} has been assigned to a bending (scissoring) vibration of methylene (CH_2) groups. These features are typical for hydrocarbon chains and reflect the fact that the compounds have similar chain fragments characterized by simple molecular structures related to hydrocarbon absorption bands at 2,921, 2,852, 1,459, and 714 cm^{-1} . There is a significant correlation exists between the images obtained at other wavenumbers, particularly those obtained at 1,375 cm^{-1} and 1,736 cm^{-1} , corresponding to cholesterol esters, which are weakly present in the paraffin spectrum. This last wavenumber is related to the C=O vibration of wax samples (Vyshniak *et al.* 2018).



Source: Elaborated by the authors.

Figure 9. FT-IR spectra of raw paraffin (crystalline) and the molten paraffin.

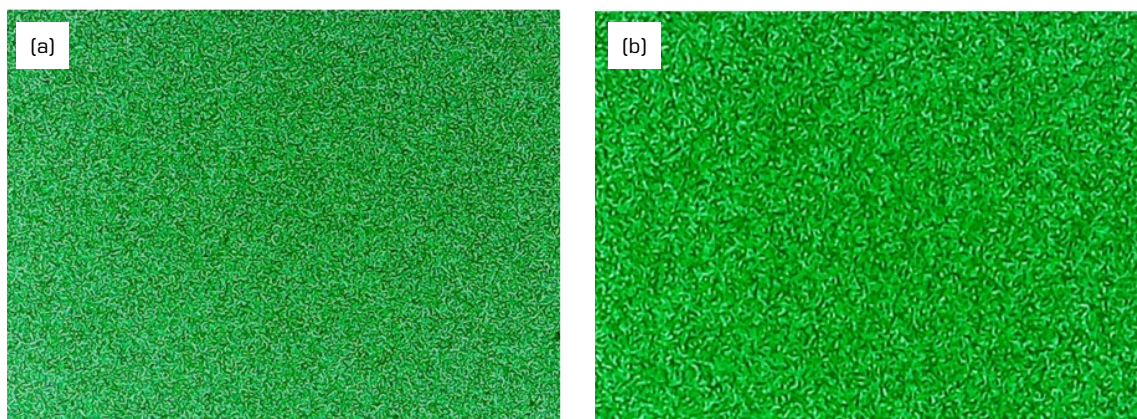
Figure 10 shows the fluorescence emission of the crystalline raw paraffin and the effect of melting once and two times. The fluorescence behavior can be related to the structural differences observed in the XRD patterns. In this case, the semicrystalline solid phase of the crystalline raw paraffin decomposes into two different solid phases when melted once or twice. The difference in the number of H and C atoms is reflected in the diminishing intensity of emission at 320, 348, and 370 nm for the crystalline raw paraffin and the molten paraffin.



Source: Elaborated by the authors.

Figure 10. Emission spectra of the raw paraffin and those subjected to one and two melting cycles.

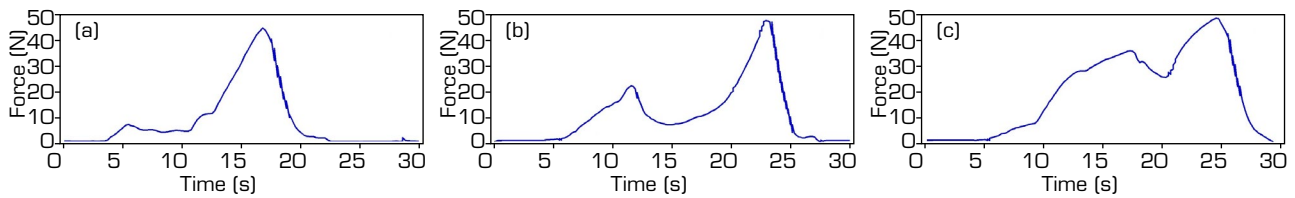
Figure 11 shows optical micrographs at two different magnifications of the paraffin-fuel unit obtained in our induction system. The unit was illuminated simultaneously with both red and green lasers in the center region of the paraffin fuel unit. This inspection method allows for obtaining structural information based on the light dispersion of the lasers used to illuminate the paraffin fuel unit. The obtained optical micrographs contain information about the inner and superficial structure of the paraffin. The optical micrographs showed a paraffin fuel unit free of internal or surface microvoids or microcracks, with high structural homogeneity.



Source: Elaborated by the authors.

Figure 11. Optical micrographs of the paraffin donuts at (a) 50x and (b) 100x.

Figure 12 shows the plastic deformation of the paraffin fuel obtained by our induction system compared with the raw crystalline paraffin and the paraffin obtained from a commercial candle. The mechanical properties were measured with a mechanical press that uses a Pasco CI6746 force sensor (-50 N – 50 N). The mechanical properties of the melted paraffin show good plasticity and resistance to fracture compared with the raw paraffin and the paraffin and the candle paraffin. The paraffin's mechanical properties and the powder's compression behavior stemming from this material can be used to estimate the compressive resistance of the paraffin fuel units. The elongation at break and the toughness of the melted paraffin increased because the agglomerated paraffin is dispersed more uniformly.



Source: Elaborated by the authors.

Figure 12. Plastic deformation for (a) raw microcrystalline paraffin, (b) commercial candle, and (c) paraffin grain obtained by the induction system.

CONCLUSION

A novel induction system utilizing an oscillating low magnetic field was successfully developed to fabricate paraffin fuel grains free of cracks and microfractures, ideal for combustion in the hybrid rocket engine designed for the Mexican Cabo Tuna space program. The physical characteristics of the system permit us adequate temperature control with a turn-on/off process of the oscillating magnetic field. The steel mold ensures a slow cooling process that produces a homogeneous paraffin without defects, which is a requirement for its application in the hybrid rocket motor. The optical, structural, and mechanical characterization of paraffin obtained by the induction system demonstrates the feasibility of producing paraffin grains with desirable properties for use as a solid propellant in hybrid rocket engines.

CONFLICT OF INTEREST

Nothing to declare.

AUTHORS' CONTRIBUTION

Conceptualization: Martínez JR, Cruz-Mendoza JA, Lobo Guerrero A, Vázquez-Martínez E; **Methodology:** Cruz-Mendoza JA, Vázquez-Martínez E, and DR Cruz; **Data Curation:** DR Cruz and González-Aguilar H; **Validation:** Lobo Guerrero A and Martínez JR; **Formal análisis:** Martínez JR, Cruz-Mendoza JA, Vázquez-Martínez E, Lobo Guerrero A, and Ortega-Zarzosa G; **Investigation:** Martínez JR, Saucedo-Zárate G, Lobo Guerrero A, and Ortega-Zarzosa G; **Resources:** González-Aguilar H, DR Cruz, and Ortega-Zarzosa G; **Writing - Original Draft:** Martínez JR, and Lobo Guerrero A; **Project administration:** Martínez JR, Saucedo-Zárate G, and Arauz-Lara JL; **Funding acquisition:** Arauz-Lara JL, and Ortega-Zarzosa G; **Final approval:** Lobo Guerrero A.

DATA AVAILABILITY STATEMENT

Data are available from the corresponding author upon reasonable request.

FUNDING

Consejo Potosino de Ciencia y Tecnología
Grant No: 23871

ACKNOWLEDGMENTS

Not applicable.

REFERENCES

- Abhat A (1983) Low temperature latent heat thermal energy storage: heat storage materials. *Sol Energy* 30(4):313-331. [https://doi.org/10.1016/0038-092X\(83\)90186-X](https://doi.org/10.1016/0038-092X(83)90186-X)
- Alkan C (2006) Enthalpy of melting and solidification of sulfonated paraffins as phase change materials for thermal energy storage. *Thermochim Acta* 451:126-130. <https://doi.org/10.1016/j.tca.2006.09.010>
- Bernard G (2013) Development of a hybrid sounding rocket motor (master's thesis). Durban: University of KwaZuluNatal, College of Agriculture, Science and Engineering.
- Bisin R, Paravan C, Alberti S, Galfetti L (2020) A new strategy for the reinforcement of paraffin-based fuels based on cellular structures: the armored grain – Mechanical characterization. *Acta Astronautica* 176:494-509. <https://doi.org/10.1016/j.actaastro.2020.07.003>
- Bucio A, Moreno-Tovar R, Bucio L, Espinosa-Dávila J, Anguebes-Franceschi F (2021) Characterization of beeswax, candelilla wax and paraffin wax for coating cheeses. *Coatings* 11:261. <https://doi.org/10.3390/coatings11030261>
- Casiano MJ, Hulka JR, Yang V (2010) Liquid-propellant rocket engine throttling: a comprehensive review. *J Propuls Power* 26(5):897-923. <https://doi.org/10.2514/1.49791>
- Caveny LH, Geisler RL, Ellis RA, Moore TL (2003) Solid rocket enabling technologies and milestones in the United States. *J Propuls Power* 19:1038-1066. <https://doi.org/10.2514/2.6944>
- Cho SY, Fogle HS (1999) Efforts on solving the problem of paraffin deposit I: using oil-soluble inhibitors. *J Ind Eng Chem* 5(2):123-127.
- Dorset DL (1995) The crystal structure of waxes. *Acta Crystallogr B* 51:1021-1028. <https://doi.org/10.1107/S0108768195005465>
- Dorset DL (2005) Crystallography of the polymethylene chain: an inquiry into the structure of waxes. Vol. 17. Oxford: Oxford University. <https://doi.org/10.1093/acprof:oso/9780198529088.001.0001>
- Gulfam R, Zhang P, Meng Z (2019) Advanced thermal systems driven by paraffin-based phase change materials – A review. *Appl Energy* 238:582-611. <https://doi.org/10.1016/j.apenergy.2019.01.114>
- Hasnain S (1998) Review on sustainable thermal energy storage technologies, part I: heat storage materials and techniques. *Energy Conserv Manag* 39:1127-1138. [https://doi.org/10.1016/S0196-8904\(98\)00025-9](https://doi.org/10.1016/S0196-8904(98)00025-9)
- Hiran S, Suwondo A, Mansoori G (1994) Characterization of alkanes and paraffin waxes for application as phase change energy storage medium. *Energy Sources* 16:117-128. <https://doi.org/10.1080/00908319408909065>
- Karabeyoglu A, Zilliack G, Cantwell BJ, De Zilwa S, Castellucci P (2004) Scale-up tests of high regression rate paraffin-based hybrid rocket fuels. *J Propuls Power* 20:1037-1045. <https://doi.org/10.2514/1.3340>
- Karabeyoglu M, Cantwell B, Altman D (2001) Development and testing of paraffin-based hybrid rocket fuels. Paper presented 2001 37th Joint Propulsion Conference and Exhibit. American Institute of Aeronautics and Astronautics; Salt Lake City, USA. <https://doi.org/10.2514/6.2001-4503>



- Kim S, Moon H, Kim J, Cho J (2015) Evaluation of paraffin-polyethylene blends as novel solid fuel for hybrid rockets. *J Propuls Power* 31:1750-1760. <https://doi.org/10.2514/1.B35565>
- Kobald M, Fischer U, Tomilin K, Petrarolo A, Schmierer C (2018) Hybrid experimental rocket Stuttgart: a low-cost technology demonstrator. *J Spacecr Rockets* 55(2):484-500. <https://doi.org/10.2514/1.A34035>
- Kumar R, Ramakrishna PA (2016) Studies on EVA-based wax fuel for launch vehicle applications. *Propellants Explos Pyrotech* 41:295-303. <https://doi.org/10.1002/prop.201500172>
- Leccese G, Cavallini E, Pizzarelli M (2019) State of art and current challenges of the paraffin-based hybrid rocket technology. Paper presented 2019 AIAA Propulsion and Energy Forum. American Institute of Aeronautics and Astronautics; Indianapolis, USA. <https://doi.org/10.2514/6.2019-4010>
- Lee EJ, Park JK, Lee YS, Lim KH (2010) Comparison of thermal properties of crude by-product polyolefin wax, fractionated paraffin wax and their blend. *Korean J Chem Eng* 27:524-530. <https://doi.org/10.1007/s11814-010-0113-y>
- Mahottamananda SN, Kadiresh PN (2019) Mechanical characteristics of paraffin wax-HTPB based hybrid rocket fuel. Paper presented 2019 International Conference of Aerospace and Mechanical Engineering. International Association of Engineers; Singapore. https://doi.org/10.1007/978-981-15-4756-0_9
- Mansoori AG, Barnes H, Webster GM (2003) Petroleum waxes. In: Totten GE, editor. *Fuels and lubricants handbook: technology, properties, performance, and testing*. 2nd ed. West Conshohocken: American Society for Testing & Materials. p. 525-556.
- Masato D, Sorgato M, Lucchetta G (2017) Prototyping and modeling of the centrifugal casting process for paraffin waxes. *Mater Manuf Process* 32:1823-1830. <https://doi.org/10.1080/10426914.2017.1317791>
- Mazzetti A, Merotto L, Pinarello G (2016) Paraffin-based hybrid rocket engines applications: a review and a market perspective. *Acta Astronautic* 126:286-297. <https://doi.org/10.1016/j.actaastro.2016.04.036>
- Okninski A (2018) On use of hybrid rocket propulsion for suborbital vehicles. *Acta Astronautic* 145:1-10. <https://doi.org/10.1016/j.actaastro.2018.01.027>
- Oztan C, Coverstone V (2021) Utilization of additive manufacturing in hybrid rocket technology: a review. *Acta Astronautic* 180:130-140. <https://doi.org/10.1016/j.actaastro.2020.11.024>
- Pal Y, Mahottamananda SN, Palateerdham SK, Subha S, Ingenito A (2021) Review on the regression rate-improvement techniques and mechanical performance of hybrid rocket fuels. *FirePhysChem* 1:272-282. <https://doi.org/10.1016/j.fpc.2021.11.016>
- Piscitelli F, Saccone G, Gianvito A, Cosentino G, Mazzola L (2015) Manufacturing processes of paraffin grains as fuel for hybrid rocket engines. Paper presented 2015 51st AIAA/SAE/ASEE Joint Propulsion Conference. AIAA/SAE/ASEE; Orlando, USA. <https://doi.org/10.2514/6.2015-4039>
- Piscitelli F, Saccone G, Gianvito A, Cosentino G, Mazzola L (2018) Characterization and manufacturing of a paraffin wax as fuel for hybrid rockets. *Propuls Power Res* 7:218-230. <https://doi.org/10.1016/j.jprr.2018.07.007>
- Risha GA, Evans B, Boyer E, Kuo K (2007) Metals, energetic additives, and special binders used in solid fuels for hybrid rockets. *Prog Astronaut Aeronaut* 218:413. <https://doi.org/10.2514/5.9781600866876.0413.0456>
- Ryan AJ, Stanford JL, Thomas WB, Nye MW (1997) A synchrotron X-ray study of melting and recrystallization in isotactic polypropylene. *Polymer* 38:759-768. [https://doi.org/10.1016/S0032-3861\(96\)00583-6](https://doi.org/10.1016/S0032-3861(96)00583-6)

- Sackheim RL (2006) Overview of United States rocket propulsion technology and associated space transportation systems. *J Propuls Power* 22:1310-1332. <https://doi.org/10.2514/1.23257>
- Saucedo-Zárate G, Arauz-Lara JL, de la Cruz-Mendoza JA, Vázquez-Martínez E, Saucedo-González MA, Lobo Guerrero A, Martínez JR (2022a) Development of a solid propellant rocket in the frame of the Cabo Tuna Mexican program. *Aerotec Missili Spazio* 101:135-141. <https://doi.org/10.1007/s42496-022-00115-8>
- Saucedo-Zárate G, Saucedo González M, Arauz Lara JL, de la Cruz Mendoza Á, Vázquez Martínez E, González Aguilar H, Martínez JR, Lobo Guerrero A (2022b) Captive-fired experiment of a solid rocket motor. *J Spacecr Rockets* 59(3):1029-1032. <https://doi.org/10.2514/1.A34999>
- Sharma SD, Sagara K (2005) Latent heat storage materials and systems: a review. *Int J Green Energy* 2:1-56. <https://www.tandfonline.com/doi/abs/10.1081/GE-200051299>
- Stober KJ, Sánchez A, Apodaca MR, Ngetich GC, Wood D (2021) Optical and thermochemical analysis for paraffin and beeswax centrifugal casting. Paper presented 2021 AIAA Propulsion and Energy Forum. AIAA. <https://doi.org/10.2514/6.2021-3504.vid>
- Tang Y, Chen S, Zhang W, Shen R, DeLuca LT, Ye Y (2017) Mechanical modifications of paraffin-based fuels and the effects on combustion performance. *Propellants Explos Pyrotech* 42:1268-1277. <https://doi.org/10.1002/prop.201700136>
- Thomas JC, Paravan C, Stahl JM, Tykol AJ, Rodriguez FA, Galfetti L, Petersen EL (2021) Experimental evaluation of HTPB/paraffin fuel blends for hybrid rocket applications. *Combust Flame*. 229:111386. <https://doi.org/10.1016/j.combustflame.2021.02.032>
- Varshney D, Ahmadi M, Guinel MJ-F, Brad Weiner R, Morell G (2012) Single-step route to diamond-nanotube composite. *Nanoscale Res Lett* 7:1-6. <https://doi.org/10.1186/1556-276X-7-535>
- Veale K, Adali S, Pitot J, Bemont C (2018) The structural properties of paraffin wax based hybrid rocket fuels with aluminium particles. *Acta Astronautic* 151:864-873. <https://doi.org/10.1016/j.actaastro.2018.07.042>
- Veale K, Adali S, Pitot J, Bemont C (2021) Explicit modelling of the ignition transient structural response of a paraffin wax hybrid rocket motor fuel grain. *J Aerosp Technol Manag* 13:e2921. <https://doi.org/10.1590/jatm.v13.1216>
- Veale K, Adali S, Pitot J, Brooks M (2017) A review of the performance and structural considerations of paraffin wax hybrid rocket fuels with additives. *Acta Astronautic* 141: 196-208. <https://doi.org/10.1016/j.actaastro.2017.10.012>
- Vyshniak V, Dimitriev O, Litvynchuk S, Dombrovskiy V (2018) Identification of beeswax and its falsification by the method of infrared spectroscopy. *Ukr Food J* 7:421-433. <https://doi.org/10.24263/2304-974X-2018-7-3-7>
- Wunderlich B (2003) The three reversible crystallization and melting processes of semicrystalline macromolecules. *Thermochim Acta* 396:33-41. [https://doi.org/10.1016/S0040-6031\(02\)00514-2](https://doi.org/10.1016/S0040-6031(02)00514-2)